BNL-113765-2017-JA

EFFECTS OF ENVIRONMENT FORCING ON MARINE BOUNDARY LAYER CLOUD-DRIZZLE PROCESSES

Wu, P., Dong, X., Xi, B., Liu, Y., Thieman, M., and Minnis, P.

Accepted for publication in
J. Geophys. Res. Atmos.

April 2017

Environmental & Climate Science Dept.

Brookhaven National Laboratory

U.S. Department of Energy
DOE Office of Science

DISCLAIMER

Effects of Environment Forcing on Marine Boundary Layer Cloud-Drizzle Processes

Peng Wu[1], Xiquan Dong[1], Baike Xi[2], Yangang Liu[3], Mandana Thieman[4], and Patrick Minnis[5]

1 Department of Hydrology and Atmospheric Sciences, University of Arizona, Tucson, AZ

2 Department of Atmospheric Sciences, University of North Dakota, Grand Forks, ND

3 Brookhaven National Laboratory, Upton, NY

4 Science Systems, and Applications, Inc., Hampton, VA

5 NASA Langley Research Center, Hampton, VA

Key words: Drizzle Formation, Vertical Wind Shear, Boundary Layer Static Instability

Revised to Journal of Geophysical Research-Atmosphere (March 24, 2017)

Main point #1: wind direction or speed shear enhances drizzle formation by broadening DSDs and increasing collision-coalescence

Main point #2: boundary layer static instability enhances drizzle formation by increasing TKE

Main point #3: boundary layer static stability decreases with increasing wind directional shear

Corresponding author address: Dr. Xiquan Dong, Department of Hydrology and Atmospheric Sciences, University of Arizona, 1118 E. 4th St. P.O. Box 210081, Tucson, AZ 85721-0081.

Email: xdong@email.arizona.edu; Phone: 520-621-4652

Abstract: Determining the factors affecting drizzle formation in marine boundary layer (MBL) clouds remains a challenge for both observation and modeling communities. To investigate the roles of vertical wind shear and buoyancy (static instability) in drizzle formation, ground-based observations from the Atmospheric Radiation Measurement (ARM) Program at the Azores are analyzed for two types of conditions. The type I clouds should last for at least five hours and more than 90% time must be non-drizzling, and then followed by at least two hours of drizzling periods while the type II clouds are characterized by mesoscale convection cellular (MCC) structures with drizzle occur every two to four hours.

By analyzing the boundary layer wind profiles (direction and speed), it was found that either directional or speed shear is required to promote drizzle production in the type I clouds. Observations and a recent model study both suggest that vertical wind shear helps the production of turbulent kinetic energy (TKE), stimulates turbulence within cloud layer, and enhances drizzle formation near the cloud top. The type II clouds do not require strong wind shear to produce drizzle. The small values of lower-tropospheric stability (LTS) and negative Richardson number (R_i) in the type II cases suggest that boundary layer instability plays an important role in TKE production and cloud-drizzle processes. By analyzing the relationships between LTS and wind shear for all cases and all time periods, a stronger connection was found between LTS and wind directional shear than that between LTS and wind speed shear.

1. Introduction

Marine boundary layer (MBL) clouds cover vast areas with the annual mean ~23% of ocean surface, making them the dominant cloud type over the oceans [*Warren et al.,* 1986, 1988; *Hahn and Warren,* 2007]. Due to their strong cooling effect on the underlying surface [*Hartmann et al.,* 1992; *Chen et al.,* 2000], only small changes in the coverage and thickness of MBL clouds could offset the radiative effects produced by increasing greenhouse gases [*Hartmann and Short,* 1980; *Randall et al.,* 1984; *Slingo,* 1990]. The lifetime of MBL clouds remains an issue in climate models [*Yoo and Li,* 2012; *Jiang et al.,* 2012; *Yoo et al.,* 2013; *Stanfield et al.,* 2014] and represents one of the largest sources of uncertainty in predicting future climate change [*Wielicki et al.,* 1995; *Houghton et al.,* 2001; *Bony and Dufresne,* 2005]. A major area of disagreement among researchers is how variations of cloud microphysical properties affect the lifetime of clouds in a warmer environment [*Cess et al.,* 1990, 1996; *Bony et al.,* 2006; *Soden and Vecchi,* 2011; *Dolinar et al.,* 2015]. It is therefore imperative to have an in-depth understanding of the physical processes that control the MBL cloud lifetime from available observations.

MBL clouds frequently produce light precipitation, usually in the form of drizzle [*Austin et al.*, 1995; *Wood*, 2005a; *Leon et al*., 2008; *Wood*, 2012; *Wu et al.,* 2015]. The effects of drizzle on the lifetime of MBL clouds are complicated. First, the latent heat released from drizzle formation warms the cloud layer, which reduces turbulent mixing, stabilizes the MBL, and induces stratification [*Nicholls,* 1984; *Stevens et al.,* 1998; *Ackerman et al.,* 2009]. Second, drizzle evaporates below cloud base, which provides an additional water vapor source for further cloud particle formation in addition to the vapor source from the environment (e.g. sea surface,

sub-cloud layer, advection, free troposphere, etc.) [*Wood,* 2005a; *Wu et al.,* 2015; *Dong et al.,* 2015].

The radiative effects of MBL clouds are determined by both micro- and macro-physical properties [*Slingo,* 1990; *Hartmann et al.,* 1992; *Dong et al.,* 1997, 1998]. Precipitation, as a regulator, plays an essential role in determining cloud properties and life cycles, thus impacting the Earth's radiation budget. *Wood* [2012] summarized the interactions between precipitation from stratocumulus clouds and other physical processes and parameters, such as turbulent kinetic energy (TKE), cloud thickness, liquid water path (*LWP*), cloud fraction, entrainment rate and cloud droplet number concentration (N_d) (Figure 26 in *Wood* [2012]). The formation of precipitation can limit cloud thickness by drying the MBL [*Lenderink and Siebesma,* 2004] and reducing TKE in the MBL by stabilization, which may also reduce the entrainment rate [*Wood,* 2007]. A precipitation rate as low as 1 mm d^{-1} is sufficient to drive down N_d by a factor of three over the remote oceans, favoring more precipitation [*Wood,* 2006; *Wood et al.,* 2012]. Although not well understood, there is evidence for precipitation driving stratocumulus breakup [*Nicholls,* 1984; *Miller and Albrecht,* 1995; *Bretherton and Wyant,* 1997; *Stevens et al., 1998*; *Comstock et al.,* 2005]. Studies have shown that drizzle tends to affect the transition from closed to open cells in regions of extensive MBL clouds [*Savic-Jovcic and Stevens,* 2008; *Wang and Feingold,* 2009]. In some instances, heavy drizzle causes the MBL to collapse to a much shallower boundary layer consisting of only a few patchy clouds or no clouds [*Christensen and Stephens,* 2011].

The initiation of precipitation/drizzle drops requires collision-coalescence of cloud droplets [*Jonas,* 1996]. Autoconversion and accretion are two processes in which specific cloud particles overcome the barrier and grow to drizzle-sized drops [*Beheng and Doms,* 1986; *Wood,*

89 2005b]. Allowing all coalescence events between cloud particles to contribute to coalescence
90 rate, *Liu and Daum* [2004] parameterized the autoconversion rate (A_c) as functions of the product
91 of cloud liquid water content (*LWC*), N_d and relative dispersion of droplet size distribution
92 (DSD). Given the greatest values of *LWC* usually occur toward the top of MBL cloud layers
93 [*Nicholls and Leighton,* 1986; *Albrecht et al.,* 1990; *Miles et al.,* 2000; *Dong et al.,* 2003; *Wood,*
94 2005a], A_c tends to reach a maximum near cloud top [*Wood,* 2005b]. In precipitating
95 stratocumulus, more precipitation drops will be generated in the accretion process than under the
96 condition of autoconversion by itself. The accretion rates, calculated from *in-situ* measurements,
97 also tend to reach a maximum in between the middle and top of cloud layers [*Wood,* 2005b].
98 Precipitation rates of MBL clouds may have strong relationships with both macro- and
99 micro-physical properties. Observations have shown that clouds with markedly different *LWP*s
100 and DSDs can have similar precipitation rates [*Austin et al.,* 1995]. That and previous studies
101 [e.g., *Baker,* 1993; *Comstock et al.,* 2004; *Xue et al.,* 2008; *Wood et al.,* 2009] found that the
102 precipitation rate near cloud base often increases with high *LWP*s and thick cloud layers, but
103 decreases with the increasing N_d [*vanZanten et al.,* 2005].
104 Earlier studies also found that the evolution of the environment may influence the
105 precipitation rate. *Nicholls* [1987] proposed that turbulence plays an essential role in
106 stratocumulus precipitation, allowing drizzle drops to form by increasing their dwell time in the
107 cloud. This idea was then further developed by *Baker* [1993] and *Austin et al.* [1995]. Those
108 studies suggested that precipitation rates might increase significantly for a doubling of the
109 vertical velocity variance. Large eddy simulations by *Feingold et al.* [1996] also showed that
110 turbulent mixing can increase the drizzle drop in-cloud residence time to enhance drizzle
111 production, thus facilitating drizzle drop growth by collision-coalescence. *Pinsky et al.* [2007]

found that turbulence can increase the collision efficiency by a factor of 4 at high flow dissipation rate. More recently, *Magaritz-Ronen et al.* [2016] used a Lagrangian-Eulerian model to simulate the effects of turbulent mixing on drizzle formation in stratocumulus clouds and found that drizzle develops only when turbulent mixing of parcels is included in the model. In this study, we investigate the impact of the turbulent mixing on the cloud-to-drizzle process using available measurements at the Department of Energy (DOE) Atmospheric Radiation Measurement (ARM) site in the Azores.

An important parameter to describe the development of turbulence is the rate of change of TKE per unit mass with time, e, and can be expressed as:

$$e = \text{shear production} + \text{buoyancy production} + \text{transport} - \text{dissipation} \quad (1)$$

Under most circumstances, buoyancy flux is the primary generator of TKE and always has a maximum value in the cloud layer [*Nicholls and Leighton,* 1986; *Moeng et al.,* 1992; *Duynkerke et al.,* 1995; *Bretherton and Wyant,* 1997]. In the stratocumulus-topped boundary layers (STBLs), which are stable with relatively weak buoyancy, the shear term can play an important or even dominant role.

Unlike previous observation/parameterization [*Nicholls,* 1987; *Baker,* 1993; *Austin et al.,* 1995] or model [*Feingold et al.,* 1996; *Magaritz-Ronen et al.,* 2016] studies, we attempt to assess the roles of vertical wind shear and boundary layer instability (buoyancy) in the drizzle initiation processes and investigate how the precipitation patterns respond to these two forcings using ground-based observations. The manuscript is organized as follows. Section 2 describes the datasets used in this study, the method used in selecting or classifying cases, and a brief description of the parameters used in the analysis. Section 3 presents the results and discussions

for two selected cases using various physical parameters as well as the statistical results from all selected cases, followed by the summary and conclusions in Section 4.

2. Data and Methods

The datasets used in this study were collected at the ARM Mobile Facility (AMF), which was deployed on the northern coast of Graciosa Island (39.09^{o}N, 28.03^{o}W) from June 2009 to December 2010 (for more details, please refer to *Rémillard et al.* [2012]; *Dong et al.* [2014a]; *Wood et al.* [2015]). The detailed operational status of the remote sensing instruments on AMF was summarized in Figure 1 of *Rémillard et al.* [2012] and discussed in *Wood et al.* [2015].

The drizzle status is identified through a combination of the W-band ARM Cloud Radar (WACR) measured reflectivity and the laser ceilometer (CEIL) detected cloud-base height [*Wu et al*. 2015]. As in *Wu et al.* [2015], we label the status of a specific time as "drizzling" if the WACR reflectivities below cloud base exceed -37 dBZ. The cloud-top heights were determined from WACR reflectivity and the cloud thickness was simply the difference between cloud top and base heights. WACR Doppler spectrum width (σ_d) was used to show the spectral broadening during drizzling. The σ_d is very sensitive to the production of drizzle-sized drops in the cloud layer and has been shown to be useful in detecting drizzle onset [*Kollias et al.,* 2011, *Luke and Kollias,* 2013].

The cloud liquid water path (*LWP)* was retrieved from the microwave radiometer (MWR) brightness temperatures measured at 23.8 and 31.4 GHz using a statistical retrieval method with an uncertainty of 20 g m^{-2} for *LWP* < 200 g m^{-2}, and 10% for *LWP* > 200 g m^{-2} [*Liljegren et al.,* 2001; *Dong et al.,* 2000]. Also retrieved from the MWR measurements is the column-integrated

precipitable water vapor (*PWV*), which gauges the total amount of water in the atmospheric column.

For all cases in this study, the cloud-top heights were below 3 km. To ensure that the ground-based point observations can represent the clouds over large areas surrounding the ARM Azores site, Meteosat-9 images were used to check the cloud areal coverage. In this study, only the cases having relatively homogeneous cloud coverage within a grid box of 6° × 7° have been selected, the cases with cloud break-up at the downstream of the ARM Azores site following the movement or with significant amount of cumulus surrounding the Azores are not included. In addition, we classified the drizzling MBL clouds into two types to better analyze the effects of vertical wind shear and buoyancy on drizzle formation. The type I clouds should last for at least five hours and more than 90% time must be labelled as "non-drizzling", and then followed by at least two hours of drizzling periods, while the type II clouds are characterized by mesoscale convection cellular (MCC) structures with drizzling periods occur every two to four hours.

As shown in Figure 1, the type I cloud (Figure 1a) is characterized by a long time of non-drizzling cloud development before intense drizzle occurred. In the type II case (Figure 1d), drizzling events occurred much more frequently than those in the type I case and the WACR reflectivity clearly showed mesoscale convection cellular (MCC) structure, which is a common arrangement of MBL clouds [*Miller and Albrecht,* 1995; *Wood and Hartmann,* 2009]. The classification is simply based on radar reflectivity but is shown to be a useful way to characterize drizzling clouds under different atmospheric conditions.

The ARM merged sounding data were generated through a combination of radiosonde, surface meteorological observation and European Centre for Medium-Range Weather Forecast (ECMWF) model output with a scaling/interpolation/smoothing scheme in order to produce

profiles of the atmospheric state in 1-min temporal and 20-m vertical resolution below 3 km [*Troyan,* 2012]. In this study, mean MBL wind speed and direction were taken from the average of the merged sounding profiles over a specific time range.

Despite its utility for quantifying eddies, TKE is difficult to calculate directly from the observations due to lack of vertical air motion data in existing observations. Instead of calculating TKE, we calculated the gradient Richardson number (R_i):

$$R_i = \frac{N^2}{U_z^2} = \frac{\frac{gd\theta}{\theta dz}}{U_z^2}, \quad (2)$$

to characterize the growth/decay of turbulence as well as the static stability of the MBL. In equation (2), N^2 is buoyancy and is calculated from the vertical gradient of potential temperature (θ), g is gravity, and U_z^2 is the square of the vertical gradient of horizontal wind speed. Previous studies have shown that non-turbulent (laminar) flow tends to shift to turbulent flow when $0 < R_i < 0.25$ [*Woods,* 1969; *Businger,* 1969]. Initially turbulent flow remains turbulent until $R_i \approx 1$ [*Woods,* 1969] and becomes non-turbulent when R_i is larger than approximately 1. The STBL is statically unstable if R_i is negative and vertical air motion is likely.

Point observations, however, are not sufficient to represent the large-scale atmospheric state, especially when trying to identify the MBL stability. To have an overview of the large-scale pattern, we calculated the lower-tropospheric stability ($LTS = \theta_{700\,hPa} - \theta_0$) for each grid within a 35° × 30° box centered at the ARM Azores site using the Modern-Era Retrospective analysis for Research and Applications, Version 2 (MERRA-2) dataset [*Rienecker et al.,* 2011]. It has a 0.5° × 0.625° spatial resolution and 25 hPa vertical resolution in the boundary layer with a maximum temporal resolution of 3 hours. The LTS for the Azores region is then represented by the average of the LTS in the 5° × 5° grid box. To check if the selected cases are in similar

aerosol regimes, we calculated the average aerosol optical depth (AOD) within a 5° × 5° grid box centered at the Azores.

3. Results and Discussions

Using the WACR reflectivity, we selected a total of 11 cases, based on the frequency of drizzle, 6 cases were classified as type I, and 5 cases were classified as type II. The dates of the cases are listed in Table 1. Out of these 11 cases, one typical case for each type was selected and presented in Figure 1 to demonstrate the roles of various parameters in drizzle formation processes.

3.1 Type I case: 27 July 2010

The clouds in this case experienced more than 10 hours of non-drizzling development before relatively intense drizzle began to occur at around 14:00 UTC. The cloud thicknesses (Figure 1b) were around 300 m with fluctuation of ±100 m. *LWP*s varied periodically and showed a similar fluctuation pattern as cloud thicknesses, *PWV* slightly varied with time and remained at an elevated level when drizzle occurred after 14:00 UTC. The Meteosat-9 images (Figures 2a and 2b) showed that the MBL cloud in this case stayed over the Azores for the entire selected time period, so it is reasonable to assume that the ground-based observations can reveal the processes of cloud development from non-drizzling to drizzling.

This case is further divided into three time periods: 01:00 to 03:00 UTC, 09:30 to 10:30 UTC and 15:00 to 19:00 UTC (denoted periods A, B and C afterwards). The averaged cloud thicknesses during A and B are nearly the same (~ 354 m) and 12 m thinner than that of the period C, while the averaged *LWP*s in periods A and B are 43 gm^{-2} higher than that in C. The

224 drizzling occurrences for these three periods, however, as shown in radar reflectivity (Figure 1a),
225 are significantly different: almost no drizzle fell out of the cloud base in A, very light drizzle is
226 evident in B, and intense drizzle occurred in C.

227 As discussed in Section 1, precipitation rate was assumed to be associated with cloud
228 thickness and *LWP* [e.g., *Baker,* 1993; *Comstock et al.,* 2004; *Xue et al.,* 2008; *Wood et al.,*
229 2009]. From the analysis of the type I MBL cloud properties, it is difficult to prove this
230 assumption because the cloud thicknesses, *LWP*s and *PWV*s during these three periods are nearly
231 the same, while their drizzling occurrences are totally different. Other factors or forcing must
232 play important roles during the transition process from cloud droplets to drizzle drops in period
233 C. Other than looking into the MBL cloud microphysical properties, we analyzed the profiles of
234 wind speed and direction from the ARM merged sounding (Figure 3). The mean wind speeds
235 (red dots) and directions (black dots) were taken from the average of the corresponding time
236 period. The horizontal wind speeds were low for all periods (less than ~ 2 m s^{-1}), suggesting that
237 the cloud layer was almost "stationary" over the Azores. Significant differences were found in
238 the profiles of mean wind direction between periods A/B and C. The changes in wind direction
239 (termed "directional shear") across the cloud layer during the periods A and B (Figures 3A and
240 3B) were much smaller than the directional shear during the period C (Figure 3C). The
241 directional shear during the period C was especially large around the cloud boundaries, leading
242 to our hypothesis that wind shear can help produce turbulence (thus TKE and mixing), enhance
243 the production of drizzle-sized drops near the cloud top, and further facilitate the conversion
244 from cloud to drizzle.

245 A recent model study by *Magaritz-Ronen et al.* [2016] provides strong support to our
246 hypothesis. In their study, a Lagrangian-Eularian model containing ~2000 air parcels advecting

247 in a turbulent-like velocity field was used to simulate a shallow marine stratocumulus cloud and
248 investigate the effect of turbulent mixing on drizzle formation. It was found that only when
249 turbulent mixing is included in the model the cloud produces drizzle (Figure 12 in *Magaritz-*
250 *Ronen et al*. [2016]). In their model simulations, the first drizzle-sized drops (termed "luck
251 parcels") form near the cloud top where the humidity is high, *LWC* values are at a maximum and
252 the cloud parcels reside long enough in the cloud to allow the formation of drizzle drops as a
253 result of efficient collisions. Although the coalescence between cloud particles was not included
254 in *Magaritz-Ronen et al.* [2016], their results are indicative and support our hypothesis.

255 Doppler spectrum width σ_d is very sensitive to cloud droplet size distributions (DSDs).
256 Large σ_d values represent a broad distribution of cloud droplets ranging from small droplets to
257 large drizzle-sized drops in the cloud, while small σ_d values denote a narrow range of DSDs,
258 representing either small cloud droplets or drizzle drops, which will be determined by radar
259 reflectivity and Doppler velocity. As shown in Figure 4, relatively large σ_d values occurred just
260 above cloud base during the periods A and B (warm colors), indicating the broad DSDs within
261 the cloud layer. Periodically changing positive and negative signs in V_d values indicates the
262 downward and upward motions within the cloud layer (Figure 4A). However, only positive V_d
263 values are seen below cloud base, indicating large drizzle drops, although σ_d values are small
264 (~10.1 UTC).

265 During the time period from 15:00 to 16:40 UTC in the period C, moderate σ_d and V_d
266 values (Figures 4C1 and 4C2), indicate a mix of cloud droplets and drizzle drops within the
267 cloud layer. Whereas relatively large V_d and reflectivity values, and small σ_d values suggest
268 drizzle occurred below cloud base. In the following period (16:45 to 17:30 UTC), large σ_d and
269 V_d values appeared in the cloud layer, suggesting a broad range of DSDs with large drizzle-sized

drops falling towards to the cloud base. Below the cloud base, large drizzle drops are dominant as demonstrated by large radar reflectivity and V_d values and small σ_d values.

Inspired by *Feingold et al.* [1996] and *Magaritz-Ronen et al.* [2016] and through an integrative analysis of the ground-based observations, we attempt to explain the mechanisms that lead to the differences in drizzling status for the periods A, B and C. During the periods A and B, several large particles form near the top of the cloud layer and start falling towards the cloud base. Due to weak wind shear, the mixing within cloud is minimal, thus providing little chance for the large particles to collect cloud droplets and fall directly out of the cloud base without any further growth. Since their particle sizes are small and number concentration is low, these particles evaporate quickly in the sub-cloud layer (especially in the period B, virga shows below the cloud base). Further drizzle formation, if any, may just repeat the above process and give little chance for intense and continuous drizzle to occur. During the period C, however, several particles not only grow to drizzle-sized drops as in the periods A and B, but also collide and collect cloud droplets due to stronger turbulent mixing induced by the vertical directional shear in the period C than in other two periods. Cloud droplets and drizzle drops during the period C have a greater chance to grow larger than in the previous two periods because of turbulently forced collision-coalescence processes. This is in agreement with previous studies [e.g., *Wang et al.,* 2005; *Pinsky et al.,* 2007]. The DSD broadening as shown in Figure 4C is also a result of turbulent effect [*Liu et al.,* 2006, 2008; *Guo et al.,* 2008; *Chandrakar et al.,* 2016].

Another role of the shear induced turbulent mixing in the drizzle formation will be the recirculation of cloud and drizzle particles within the cloud layer as proposed by *Feingold et al.* [1996] and *Magaritz et al.* [2009]. Instead of falling out of the cloud base, the drizzle drops are recirculated in the cloud layer, allowing longer residence time for those drops to grow large

293 enough by collecting cloud droplets or other drizzle drops. Until the buoyancy and turbulence
294 force can no longer sustain the drizzle drops' weight, they fall out of the cloud base. The
295 enhanced collision-coalescence process indeed allows the particles to grow much larger and
296 stimulate drizzle production afterwards; this can be visualized from the radar measurements
297 shown in Figures 1a and 4 where the drizzling event during the period C can last for more than 6
298 hours. These discussions are in general agreement with *Magaritz-Ronen et al.* [2016], who
299 determined two main phases of drizzle formation. First, large drops form in the most adiabatic
300 parcels within the cloud layer, which are usually near cloud top, and turbulent mixing then leads
301 to further formation of more large particles and drizzle sized drops. In this study, the only
302 difference between the periods A/B and C we found is the directional shear, especially around
303 the cloud top - this is the primary TKE production term in equation (1) for this case, which
304 results in non-drizzle (periods A and B) and drizzling occurrences (period C).
305
306 **3.2 Type II case: 22 November 2009**
307 The Meteosat-9 images (Figures 2c and 2d) show a fast-moving cloud field with closed
308 cell MCC structures, which is similar to that presented in *Wood and Hartmann* [2009]. Although
309 the ground-based observations cannot directly capture the bright and dark stripes as seen in the
310 Meteosat-9 images, the fluctuation of cloud properties, such as cloud thickness, *LWP* and *PWV*
311 (Figure 1f), between cells correspond well with the bright and dark strips. In details, the lower
312 radar reflectivity, thinner cloud layer, and less *LWP* and *PWV* correspond well to the dark strips
313 (lower cloud albedo from satellite visible observations), while the higher radar reflectivity,
314 thicker cloud layer and higher *LWP* and *PWV* match well with bright stripes (higher cloud
315 albedo). Meanwhile, the MCC structure can also be clearly visualized from the radar reflectivity

316 shown in Figure 1d and corresponds well with drizzle that occurs every 2 to 4 hours. In general,
317 the cloud layers are relatively thick and the cloud *LWP* and *PWV* values are higher during the
318 drizzling periods than those during non-drizzling periods. Note, that the *PWV* values in this case
319 are only half of those in the type I, presumably due to the seasonal variation between summer
320 (type I case) and autumn (type II case).

321 Figure 5 shows the profiles of wind speed and direction using ARM merged sounding
322 data, a similar analysis to the type I case. Due to the similar cloud-drizzle structure for each cell
323 in this case, four time periods were selected to demonstrate their mean wind profiles in Figure 5.
324 The four time periods are: (A) 02:00 to 05:00 UTC, (B) 06:00 to 08:00 UTC, (C) 14:00 to 18:00
325 UTC and (D) 18:00 to 22:00 UTC. The profiles of wind speed and direction for all four periods
326 appear to be very similar to each other despite different cloud base and top heights. No strong
327 vertical variations have been found in both wind speed and direction. This is in contrast to the
328 results of the type I case in which strong directional wind shear exists around the cloud top
329 during intense drizzling periods. The wind speeds in the type II case are two to four times higher
330 than those in the type I case, which is consistent with the fast-moving cloud field in the
331 Meteosat-9 images.

332 In addition to comparing only the selected periods in the type I and type II cases, the time
333 series of maximum directional wind shear within the cloud layer is shown in Figure 6. The
334 directional shear was calculated from the difference of wind direction between two adjacent
335 layers (every 20 m) and the maximum value in each column within the cloud layer was selected
336 and shown in Figure 6. The directional shears in the type II case were generally smaller than
337 those in the type I case, except for several large values around 06:00 UTC. The extensive strong

338 directional wind shear from 14:00 to 20:00 UTC in the type I case corresponds well with its
339 intense drizzling period as shown in Figures 1 and 4.

340 The lack of strong wind shears in the type II case seems to contradict our hypothesis
341 proposed in the type I case. However, in equation (1), the TKE production is a combined effect
342 of shear and buoyancy effects. With the absence of shear production, the buoyancy production
343 term will be the primary forcing to generate TKE. To confirm this, we calculated LTS using
344 MERRA-2 reanalysis for the two cases every three hours (Figures 7 and 8) where smaller LTS
345 values indicate relatively stronger instability. Figure 8 shows that the LTS values in type II case
346 are much smaller than those in the type I case (Figure 7), suggesting that the type II case has
347 stronger instability and upward air motion and the buoyancy term dominates the TKE
348 production, leading to the periodic drizzling events in the type II case. When drizzle falls out
349 cloud base, these drops will evaporate and generate cold pools, which will reduce TKE within
350 the MBL by stabilization. Turbulence then becomes weak or tends to decay. With less water
351 vapor being transported upward, drizzle strength would be reduced. This process corresponds to
352 the non-drizzling or light drizzling periods in Figure 1d. After that, buoyancy due to large-scale
353 static instability induces the production of TKE again and promotes drizzle production. The
354 repeated buoyancy-drizzling-stabilization-non-drizzling processes, similar to the roles of
355 precipitation-generated oscillations in MBL cloud structures proposed by *Feingold et al.* [2010],
356 may be one of the mechanisms that leads to the commonly seen MCC structures and periodic
357 drizzling events in MBL stratocumulus clouds.

358 The large-scale patterns in both Figures 7 and 8 also show distinct differences: for the
359 type I case, the LTS values increase from the Azores to the edge of the box (eastward), while for
360 the type II case, the LTS values decrease from the Azores to the edge of the grid box (eastward).

361 This also suggests that the boundary layer in the type II case was less stable than in the type I
362 case. The LTS gradient (west-east, not show) also exhibited different patterns for the two cases:
363 the gradients around the Azores in the type I case were ~0.4 K/deg eastward while they were
364 nearly zero in the type II case. However, as shown in Figure 3, the wind speed in the type I case
365 was low, so the strong LTS gradient around the Azores did not induce strong wind speed, but
366 strong directional change.

367 To better demonstrate the dominant factors that control drizzle formation for the two
368 types of drizzling clouds, we calculated the gradient Richardson number (R_i Figure 9) and the
369 average R_i profiles in and near the cloud layers for the two cases for the same time periods as in
370 Figure 3 and 5. R_i can be an indicator of both wind shear (denominator in equation (2)) and
371 boundary layer stability (nominator in equation (2)) where negative R_i indicate unstable
372 boundary layer. In the type I case, (upper panel of Figure 9), several layers of negative R_i below
373 cloud base are probably due to small scale (~20 m) thermodynamic instability caused by the
374 evaporation of several small drizzle-sized drops. Layers just beneath cloud top during the period
375 15:00-19:00 UTC (Figure 9C) indicate the existence or production of turbulence and correspond
376 well with both the strong directional shear near cloud top (Figure 3C) and the intense drizzle
377 during this period (Figure 1a). In contrast, the turbulence in the previous two periods (Figures 9a
378 and 9b) is very weak, almost no turbulent mixing near the cloud tops during the periods A and B.
379 The differences in R_i among these three periods, again, prove the validity of the hypothesis
380 proposed for the type I case. The colored dots below cloud base in Figure 9C indicate the
381 production of turbulence, but do not necessarily enhance the turbulence intensity. We suspect
382 that the production of turbulence below cloud base in the period C is caused by the drag force of
383 hydrometers falling towards the surface, but a further study is needed to verify it.

384 The R_i values in the type II case are significantly different from those in the type I case.
385 Almost no turbulence exists to enhance drizzle formation near the cloud top in the type II case.
386 This suggests a different mechanism of drizzle formation processes between two cases. Some
387 degree of turbulence exists in the middle and lower part of the cloud layers. It, however,
388 contributes little to drizzle production because the largest particles and air parcels containing
389 highest *LWC* usually reside near the cloud top. A notable feature is the negative R_i values below
390 cloud base, suggesting the extensive static instability and hence the existence of buoyancy in the
391 type II case, which is consistent to the low LTS around the Azores as shown in Figure 8. With a
392 stronger buoyancy force in the vertical direction, particles in the type II case can grow larger
393 than those in the type I case without falling out of the cloud base. This may be one of the reasons
394 that with much lower *PWV* in the type II case, the *LWP*s and cloud thicknesses during drizzling
395 are comparable to the values in the type I case.

396 It is important to note that we are not suggesting that directional shear is the only factor
397 promoting drizzle production for type I clouds. As we will show next, either the directional shear
398 or speed shear is required to stimulate drizzle production in non-drizzling clouds that experience
399 several hours of development. Conversely, we are not suggesting that wind shear is unimportant
400 or does not occur in the type II drizzling clouds. As we will show in the statistical results below,
401 moderate directional or speed shears may also exist in type II clouds, but the values are smaller
402 than those found in the type I clouds and the dominant factor attributing to TKE production in
403 type II clouds in equation (1) is the buoyancy term. Though two cases discussed above are from
404 two seasons (summer and fall), seasonal variations will not affect our conclusions of drizzle
405 formation, as will be discussed in next section. These two cases represent typical cloud-drizzle
406 processes where the type I case is relatively static over the Azores during the entire period while

the type II case is moving straightly southeastwards. To evaluate the effect of cloud movement on cloud-drizzle processes, we also checked MetroSat-9 RGB images for the case of November 3rd, 2009 (not show), which is the second case in Figure 10 as will discuss below. This is a type I cloud and is also moving southeastward. As shown in Table 1 and Figure 10, the primary forcing in generating TKE is wind shear in this case. Despite similar cloud movement, the dominant forcing in cloud-drizzle processes in the November 3rd, 2009 case is different from the November 22nd, 2009 case. It is the wind shear, rather than absolute wind speed and/or direction, that promotes drizzle formation.

3.3 Statistics from All Cases

A total of 11 cases have been selected to perform the statistical analysis in this study, six cases are classified as type I, and five as type II (Table 1). From Meteosat-9 images of all cases (not shown), all the type I cases have relatively homogeneous cloud fields except when the clouds tend to break up at the end of the series, and all the type II cases have obvious MCC structures except for the case of 20100412 in which the MCC structure is not obvious during the first five hours. Daily averaged AODs from MERRA-2 (Figure 10c) show that all cases are under typical MBL aerosol regimes (AOD < 0.2 and Figure 2a of *Logan et al*. 2014) and no Saharan dust outbreak or heavy pollution transportations (0.25<AOD<0.52, Table 1 in *Logan et al.* 2014). Since drizzle drops normally form near the cloud top, we use the wind direction and speed in layers 100 m just above and below the cloud top for the statistical analysis of vertical wind shears.

The wind directional and speed shears during drizzling periods is shown in Figure 10. Although the median and upper quartile values for some of the type II cases are as high as those

in the type I cases, the averaged wind directional and speed shears from the type I cases are much larger than those of the type II cases (Table 1 and black dots in Figure 10). The lower to upper quartile ranges for the type I cases are, in general, larger than those for the type II cases, suggesting relatively inhomogeneous wind fields in the type I cases during drizzling periods. The 5^{th} and 7^{th} cases are the types I and II cases we selected to show, respectively, and the wind shears agree well with the wind profiles (Figures 3 and 5). As mentioned above, not all type I cases have strong directional shear. For example, the 2^{nd}, 3^{rd} and 4^{th} cases have relatively weak directional shear compared with other type I cases, but their speed shear is higher. Some cases, for example the 1^{st} and 6^{th} cases, have both strong directional and speed shears. This leads us to conclude that, for factors of wind directional shear and speed shear, at least one of them is required to exist near the cloud top to favor drizzle production in a stable MBL cloud. For the type II cases, moderate vertical wind shears may also exist, for example the 11^{th} case, but are not necessary for drizzle production. For the type II cases with weak directional and speed shears, their LTS values are usually lower (Table 1 and Figure 11). Thus, they can generate sufficient buoyancy forcing to compensate for the reduction of the shear production term in equation (1) and keep TKE at a level high enough to promote drizzle production. The 8^{th} and 9^{th} cases are examples in which both the directional and speed shears are weak even when compared with other type II cases, but their corresponding LTS values are the lowest among all cases (Table 1).

Figure 11 shows the relationships between LTS and directional shear (Figure 11a) and speed shear (Figure 11b) of all cases and for all time periods (non-drizzling and drizzling). The LTS values for type II cases are generally lower than those for type I cases, indicating the dominant role of buoyancy in TKE production and promotion of drizzle formation. Although the number of cases is limited, a rough estimate of the boundary layer LTS necessary to separate the

two types is 19 K. In other words, when LTS is below 19 K, the buoyancy plays a relatively important role in drizzle production for MBL clouds at the Azores. All the trend lines, except for the relationship between LTS and directional shear for type II cases, have negative slopes, indicating that LTS decreases with increasing wind shear. This is physically reasonable because the boundary layer will be less stable when the vertical shear becomes stronger. The positive slope between LTS and directional shear for type II cases is due to LTS and directional shear covering only a very small range (less than 0.4 deg m^{-1}) and, hence, cannot fully represent the relationship of LTS and larger variations of directional shears (e.g. 0-3.0 deg m^{-1} in Figure 11a). The relationship between LTS and directional shear for type I cases has the highest correlation coefficient (0.38), suggesting that the boundary layer stability has a stronger connection with the changes in wind direction than with the changes in wind speed. The distribution of the circles for drizzling periods (circles with solid centers) is very similar to that for all time periods, this further indicates the generality of the statistical relationships between LTS and vertical wind shears.

The factors that affect drizzle formation in MBL clouds investigated in this study are environmental variables; the role of cloud microphysical properties is beyond the scope of this study. However, as discussed in Section 1 and previous studies, precipitation rate varies significantly with N_d (and cloud thickness and *LWP*) [*Bretherton et al.,* 2004; *Wood,* 2005a; *Lu et al.,* 2007] and *LWC* [*Xue et al.,* 2008]. Environmental factors, such as aerosol number concentration and chemical properties, may also change precipitation rate substantially. And the environmental factors and microphysical properties may be coupled to one another as well. In this study, we attempted to use only cloud layers appearing to be homogeneous and having nearly the same properties during drizzling periods to the best of our knowledge, in order to

476 isolate the environmental effects from cloud microphysical effects and examine them separately.
477 With the cloud microphysical properties reported by *Dong et al.* [2014 a&b], our next step is to
478 investigate the effects of varying microphysical properties on drizzle production.
479
480 **4. Summary and Conclusions**
481 To investigate the roles of vertical wind shear and buoyancy (static instability) in drizzle
482 formation, ground-based observations from the ARM site in the Azores were analyzed for two
483 types of conditions. Type I clouds are those that developed for several hours before intense
484 drizzle occurred, while the type II clouds are characterized by mesoscale convection cellular
485 (MCC) structures with more frequent drizzle occurrence.
486 By analyzing the boundary layer wind profiles (direction and speed), it is found that in
487 type I clouds, either directional shear or speed shear is required to promote drizzle production,
488 but is not necessarily required for type II clouds. The hypothesis for the wind shear effect is that
489 vertical wind shear helps the production of TKE and enhances drizzle formation near cloud top.
490 This hypothesis is in general agreement with a recent model study by *Magaritz-Ronen et al.*
491 [2016]. Physical explanation of the hypothesis is straightforward. The largest cloud particles and
492 air parcels with highest *LWC* reside near the cloud top. The existence of vertical wind shear
493 (directional, speed, or both) enhances TKE and recirculates the particles in the cloud layer. With
494 increased residence time, those large particles have a greater chance to collect other particles,
495 grow to drizzle sized drops and then fall out as drizzle fluxes indicated in radar reflectivities
496 below cloud base.
497 Different from the wind profiles in type I clouds, type II clouds do not require strong
498 wind shear during drizzling periods. The layers below cloud base for type II are characterized by

499 negative R_i, showing lower static stability. The relatively low static stability is strong enough to
500 compensate for the reduction of wind shear and helps the production of TKE and stimulates
501 drizzle formation. Precipitation can reduce TKE, but the large-scale forcing is favorable for
502 buoyancy, thus resulting in periodic drizzling events, causing the cloud layer to have the MCC
503 structure.

504 A critical LTS value (19 K) is drawn from the statistics of all cases, below which the
505 dominant TKE production term would be buoyancy (type II) and above which would be the
506 shear term. The boundary layer stability is found to have a stronger relationship with wind
507 directional shears than with speed shears.

508 The impacts of other environmental factors (e.g., aerosol etc.) and cloud microphysical
509 properties (e.g., particle size, number concentration etc.) to drizzle formation are not included in
510 this study though they may hold similar importance. The next step of our study will be looking
511 into the cloud microphysical properties and examine their roles in the cloud-drizzle processes.

512

513 **Acknowledgments**

514 The ground-based measurements were obtained from the Atmospheric Radiation
515 Measurement (ARM) Program sponsored by the U.S. Department of Energy (DOE) Office of
516 Energy Research, Office of Health and Environmental Research, Environmental Sciences
517 Division. The data can be downloaded from http://www.archive.arm.gov/. The Meteosat-9
518 images were obtained from the SatCORPS website at NASA Langley Research Center
519 (http://satcorps.larc.nasa.gov/AMF-AZORES) sponsored by ASR project under grant DE-
520 SC0000991. The Modern-Era Retrospective analysis for Research and Applications, Version 2
521 (MERRA-2) date can be downloaded from

http://disc.sci.gsfc.nasa.gov/uui/datasets?keywords=%22MERRA-2%22. This research was supported by the DOE CESM project under grant DE-SC0014641 at University of Arizona through subaward from University of Maryland at Baltimore County, and NASA CERES project under grant NNX17AC52G at University of Arizona. Dr. Liu is supported by the DOE ASR program.

528 **References:**

529 Ackerman, A. S., M.. C. vanZanten, B. Stevens, V. Savic-Jovcic, C. S. Bretherton, A. Chlond, J.
530 Golaz, Hongli Jiang, M. Khairoutdinov, S. K. Krueger, D. C. Lewellen, A. Lock, C. Moeng,
531 K. Nakamura, M. D. Petters, J. R. Snider, S. Weinbrecht, and M. Zulauf (2009), Large-eddy
532 simulations of a drizzling, stratocumulus-topped marine boundary layer, *Mon. Wea. Rev.,*
533 *137,* 1083–1110.

534 Albrecht, B. A., C. W. Fairall, D. W. Thomson, A. B. White, J. B. Snider, and W. H. Schubert
535 (1990), Surface-based remote sensing of the observed and the adiabatic liquid water content
536 of stratocumulus clouds, *Geophys. Res. Lett., 17,* 89–92.

537 Austin, P., Y. Wang, R. Pincus, and V. Kujala (1995), Precipitation in stratocumulus clouds:
538 Observations and modelling results, *J. Atmos. Sci., 52*, 2329–2352.

539 Baker, M. B. (1993), Variability in concentrations of cloud condensation nuclei in the marine
540 cloud-topped boundary layer, *Tellus, 45B,* 458–472.

541 Beheng, K. D., and G. Doms (1986), A general formulation of collection rates of cloud and
542 raindrops using the kinetic equation and comparison with parameterizations, *Beitr. Phys.*
543 *Atmos., 59,* 66–84.

544 Bony, S., and J.-L. Dufresne (2005), Marine boundary layer clouds at the heart of tropical cloud
545 feedback uncertainties in climate models, *Geophys. Res. Lett., 32,* L20806,
546 doi:10.1029/2005GL023851.

547 Bony, S. R. Colman, V. M. Kattsov, R. P. Allan, C. S. Bretherton, J. Dufresne, A. Hall, S.
548 Hallegatte, M. M. Holland, W. Ingram, D. A. Randall, B. J. Soden, G. Tselioudis, and M. J.
549 Webb (2006), How well do we understand and evaluate climate change feedback processes?
550 *J. Clim., 19,* 3445–3482.

551 Bretherton, C. S., and M. C. Wyant (1997), Moisture transport, lower-tropospheric stability, and
552 decoupling of cloud-topped boundary layers, *J. Atmos. Sci., 54,* 148–167.
553 Bretherton, C. S., T. Uttal, C. W. Fairall, S. E. Yuter, R. A. Weller, D. Baumgardner, K.
554 Comstock, and R. Wood (2004), The EPIC 2001 stratocumulus study. *Bull. Amer. Meteor.*
555 *Soc., 85,* 967–977.
556 Businger, J. A. (1969), Note on the critical Richardson number(s), *Quart. J. Roy. Meteor. Soc.,*
557 95, 653–654, doi:10.1002/qj.49709540519.
558 Cess, R. D., G. L. Potter, J. P. Blanchet, G. J. Boer, A. D. Del Genio, M. Déqué, V. Dymnikov,
559 V. Galin, W. L. Gates, S. J. Ghan, J. T. Kiehl, A. A. Lacis, H. Le Treut, Z.-X. Li, X.-Z.
560 Liang, B. J. McAvaney, V. P. Meleshko, J. F. B. Mitchell, J.-J. Morcrette, D. A. Randall, L.
561 Rikus, E. Roeckner, J. F. Royer, U. Schlese, D. A. Sheinin, A. Slingo, A. P. Sokolov, K. E.
562 Taylor, W. M. Washington, R. T. Wetherald, I. Yagai, and M.-H. Zhang (1990),
563 Intercomparison and interpretation of climate feedback processes in 19 atmospheric general
564 circulation models, *J. Geophys. Res., 95,* 16 601–16 615, doi:10.1029/JD095iD10p16601.
565 Cess, R. D., M. H. Zhang, W. J. Ingram, G. L. Potter, V. Alekseev, H. W. Barker, E. Cohen-
566 Solal, R. A. Colman, D. A. Dazlich, A. D. Del Genio, M. R. Dix, V. Dymnikov, M. Esch, L.
567 D. Fowler, J. R. Fraser, V. Galin, W. L. Gates, J. J. Hack, J. T. Kiehl, H. Le Treut, K. K.-W.
568 Lo, B. J. McAvaney, V. P. Meleshko, J.-J. Morcrette, D. A. Randall, E. Roeckner, J.-F.
569 Royer, M. E. Schlesinger, P. V. Sporyshev, B. Timbal, E. M. Volodin, K. E. Taylor, W.
570 Wang, and R. T. Wetherald (1996), Cloud feedback in atmospheric general circulation
571 models: An update, *J. Geophys. Res., 101,* 12791–12794, doi:10.1029/96JD00822.
572 Chandrakar K. K., W. Cantrell, K. Chang, D. Ciochetto, D. Niedermeier, M. Ovchinnikov, R. A.
573 Shaw and F. Yang (2016), Aerosol indirect effect from turbulence-induced broadening of

574 cloud droplet size distributions, *Proc. Natl. Acad. Sci. U.S.A.,* doi:
575 10.1073/pnas.1612686113.
576 Chen, T., W. B. Rossow, and Y. C. Zhang (2000), Radiative effects of cloud-type variations, *J.*
577 *Climate, 13,* 264–286.
578 Christensen, M. W., and G. L. Stephens (2011), Microphysical and macrophysical responses of
579 marine stratocumulus polluted by underlying ships: Evidence of cloud deepening, *J.*
580 *Geophys. Res., 116,* D03201, doi:10.1029/2010JD014638.
581 Comstock, K., R. Wood, S. Yuter, and C. S. Bretherton (2004), Radar observations of
582 precipitation in and below stratocumulus clouds, *Quart. J. Roy. Meteor. Soc., 130,* 2891-
583 2918.
584 Comstock, K., C. S. Bretherton, and S. Yuter (2005), Mesoscale variability and drizzle in
585 southeast Pacific stratocumulus, *J. Atmos. Sci., 62,* 3792–3807.
586 Dolinar, E., X. Dong, and B. Xi (2015), Evaluation and Intercomparison of Clouds, Precipitation,
587 and Radiation Budgets in Recent Reanalyses using Satellite-Surface Observations, *Climate*
588 *Dyn.,* DOI: 10.1007/s00382-015-2693-z.
589 Dong X., T.P. Ackerman, E.E. Clothiaux, Pilewskie, and Y. Han (1997), Microphysical and
590 Radiative Properties of Stratiform Clouds Deduced from Ground-based Measurements, *J.*
591 *Geophys. Res, 102,* 23829-23843.
592 Dong X., T.P. Ackerman, and E.E. Clothiaux (1998), Parameterizations of Microphysical and
593 Radiative Properties of Boundary Layer Stratus from Ground-based measurements, *J.*
594 *Geophys. Res. 102,* 31,681-31,393.

595 Dong, X., P. Minnis, T. P. Ackerman, E. E. Clothiaux, G. G. Mace, C. N. Long, and J. C.
596 Liljegren (2000), A 25-month database of stratus cloud properties generated from ground-
597 based measurements at the ARM SGP site, *J. Geophys. Res. 105,* 4529-4538.
598 Dong, X., and G. G. Mace (2003), Profiles of low-level stratus cloud microphysics deduced from
599 ground-based measurements, *J. Atmos. Oceanic Technol., 20,* 42–53, doi:10.1175/1520-
600 0426(2003)020,0042:POLLSC.2.0.CO;2.
601 Dong, X., B. Xi, A. Kennedy, P. Minnis and R. Wood (2014a), A 19-month Marine Aerosol-
602 Cloud_Radiation Properties derived from DOE ARM AMF deployment at the Azores: Part
603 I: Cloud Fraction and Single-layered MBL cloud Properties, *J. Climate, 27*,
604 doi:10.1175/JCLI-D-13-00553.1.
605 Dong, X., B. Xi, and P. Wu (2014b), Investigation of Diurnal Variation of MBL Cloud
606 Microphysical Properties at the Azores, *J. Climate, 27*, 8827-8835.
607 Dong, X., A. Schwantes, B. Xi and P. Wu (2015), Investigation of the Marine Boundary Layer
608 Cloud Properties under Coupled and Decoupled Conditions at the Azores, *J. Geophys. Res.,*
609 *120*, 6179–6191, doi:10.1002/2014JD022939.
610 Duynkerke, P. G., H. Q. Zhang, and P. J. Jonker (1995), Microphysical and turbulent structure of
611 nocturnal stratocumulus as observed during ASTEX, *J. Atmos. Sci., 52,* 2763–2777.
612 Feingold, G., W. Cotton, B. Stevens, and A. S. Frisch (1996), The relationship between drop in-
613 cloud residence time and drizzle production in numerically simulated stratocumulus clouds,
614 *J. Atmos. Sci., 53,* 1108–1122.
615 Feingold, G., I. Koren, H. Wang, H. Xue, and W. A. Brewer (2010), Precipitation-generated
616 oscillations in open cellular cloud fields, *Nature, 466(7308),* 849–852,
617 doi:10.1038/nature09314.

618 Guo, H, Y. Liu and J. Penner (2008), Does threshold representation associated with the
619 autoconversion process matter? *Atmos. Chem. Phys., 8,* 1225-1230.
620 Hahn, C. J., and S. G. Warren (2007), A gridded climatology of clouds over land (1971–96) and
621 ocean (1954–97) from surface observations worldwide, Numeric Data Package NDP-
622 026EORNL/CDIAC-153, CDIAC, Department of Energy, Oak Ridge, TN.
623 Hartmann, D. L., and D. Short (1980), On the use of earth radiation budget statistics for studies
624 of clouds and climate, *J. Atmos. Sci., 37,* 1233–1250.
625 Hartmann, D. L., M. E. Ockert-Bell, and M. L. Michelsen (1992), The effect of cloud type on
626 earth's energy balance—Global analysis, *J. Climate, 5,* 1281–1304.
627 Houghton, J. T., Y. Ding, D.J. Griggs, M. Noguer, P.J. van der Linden, X. Dai, K. Maskell,
628 and C.A. Johnson (2001), Climate Change: The Scientific Basis, *Cambridge University*
629 *Press*, 881 pp.
630 Jiang, J., H. Su, C. Zhai, V. S. Perun, A. Del Genio, L. S. Nazarenko, L. J. Donner, L. Horowitz,
631 C. Seman, J. Cole, A. Gettelman, M. A. Ringer, L. Rotstayn, S. Jeffrey, T. Wu, F. Brient, J-
632 L. Dufresne, H. Kawai, T. Koshiro, M. Watanabe, T. S. LÉcuyer, E. M. Volodin, T. Iversen,
633 H. Drange, M. D. S. Mesquita, W. G. Read, J. W. Waters, B. Tian, J. Teixeira, and G. L.
634 Stephens (2012), Evaluation of cloud and water vapor simulations in CMIP5 climate models
635 using NASA ''A-train'' satellite observations, *J. Geophys. Res., 117,* D14105,
636 doi:10.1029/2011JD017237.
637 Jonas, P. R. (1996), Turbulence and cloud microphysics, *Atmos. Res., 40,* 283–306.
638 Kollias, P., J. Rémillard, E. Luke, and W. Szyrmer (2011), Cloud radar Doppler spectra in
639 drizzling stratiform clouds: 1. Forward modeling and remote sensing applications, *J.*
640 *Geophys. Res., 116,* D13201, doi:10.1029/2010JD015237.

641 Lenderink, G., and A. P. Siebesma (2004), On the role of drizzle in stratocumulus and its
642 implications for large-eddy simulation, *Quart. J. Roy. Meteor. Soc., 130,* 3429–3434.
643 Leon, D. C., Z. Wang, and D. Liu (2008), Climatology of drizzle in marine boundary layer
644 clouds based on 1 year of data from CloudSat and Cloud-Aerosol Lidar and Infrared
645 Pathfinder Satellite Observations (CALIPSO), *J. Geophys. Res., 113*, D00A14,
646 doi:10.1029/2008JD009835.
647 Liljegren, J. C., E. E. Clothiaux, G. G. Mace, S. Kato, and X. Dong (2001), A new retrieval for
648 cloud liquid water path using a ground-based microwave radiometer and measurements of
649 cloud temperature, *J. Geophys. Res*., *106,* 14,485-14,500.
650 Liu, Y., and P. H. Daum (2004), On the parameterization of the autoconversion process. Part I:
651 Analytical formulation of the Kessler-type parameterizations, *J. Atmos. Sci.,* 61, 1539–1548.
652 Liu, Y., P. H. Daum, R. McGraw, and M. Miller (2006), Generalized threshold function
653 accounting for effect of relative dispersion on threshold behavior of autoconversion process.
654 *Geophys. Res. Lett, 33,* L11804, doi:10.1029/2005GL0255000.
655 Liu, Y., B. Geert, M. Miller, P. H. Daum, and M. McGraw (2008), Threshold radar reflectivity
656 for drizzling clouds. *Geophys. Res. Lett, 35,* L03807, doi:10.1029/2007GL031201.
657 Logan, T., B. Xi, and X. Dong (2014), Aerosol properties and their influences on marine
658 boundary layer cloud condensation nuclei at the ARM mobile facility over the Azores, *J.*
659 *Geophys. Res. Atmos.*, 119, 4859-4872, doi:10.1002/2013JD021288.
660 Lu, M. L., W. C. Conant, H. H. Jonsson, V. Varutbangkul, R. C. Flagan, and J. H. Seinfeld
661 (2007), The Marine Stratus/Stratocumulus Experiment (MASE): Aerosol-cloud
662 relationships in marine stratocumulus. *J. Geophys. Res., 112,* D10209,
663 doi:10.1029/2006JD007985.

664 Luke, E. P., and P. Kollias (2013), Separating cloud and drizzle radar moments during
665 precipitation onset using Doppler spectra, *J. Atmos. Oceanic Technol., 30,* 1656–1671.
666 Magaritz-Ronen, L., M. Pinsky, and A. Khain (2016), Drizzle formation in stratocumulus clouds:
667 effects of turbulent mixing, *Atmos. Chem. Phys., 16,* 1849-1862, doi:10.5194/acp-16-1849-
668 2016.
669 Miles, N. L., J. Verlinde, and E. E. Clothiaux (2000), Cloud-droplet size distributions in low-
670 level stratiform clouds, *J. Atmos. Sci., 57,* 295–311, doi:10.1175/1520-0469(2000)057,0295:
671 CDSDIL.2.0.CO;2.
672 Miller, M. A., and B. A. Albrecht (1995), Surface-based observations of mesoscale cumulus-
673 stratocumulus interaction during ASTEX, *J. Atmos. Sci., 52,* 2809–2826.
674 Moeng, C. H., S. H. Shen, and D. A. Randall (1992), Physical processes within the nocturnal
675 stratus-topped boundary layer, *J. Atmos. Sci., 49,* 2384–2401.
676 Nicholls, S. (1984), The dynamics of stratocumulus: Aircraft observations and comparisons with
677 a mixed layer model, *Quart. J. Roy. Meteor. Soc., 110,* 783–820.
678 Nicholls, S. (1987), A model of drizzle growth in warm, turbulent, stratiform clouds, *Quart. J.*
679 *Roy. Meteor. Soc., 113,* 1141–1170.
680 Nicholls, S., and J. Leighton (1986), An observational study of the structure of stratiform cloud
681 sheets: Part I. Structure, Quart. *J. Roy. Meteor. Soc., 112,* 431–460.
682 Pinsky, M. B., A. P. Khain, M. Shapiro (2007), Collisions of cloud droplets in a turbulent flow.
683 Part IV: droplet hydrodynamic interaction. *J. Atmos. Sci. 64*:2462‑82.
684 Randall, D. A., and M. J. Suarez (1984), On the dynamics of stratocumulus formation and
685 dissipation, *J. Atmos. Sci., 41,* 3052–3057.

686 Rienecker M. M., M. M. Rienecker, M. J. Suarez, R. Gelaro, R. Todling, J. Bacmeister, E. Liu,
687 M. G. Bosilovich, S. D. Schubert, L. Takacs, G-K. Kim, S. Bloom, J. Chen, D. Collins, A.
688 Conaty, A. da Silva, W. Gu, J. Joiner, R. D. Koster, R. Lucchesi, A. Molod, T. Owens, S.
689 Pawson, P. Pegion, C. R. Redder, R. Reichle, F. R. Robertson, A. G. Ruddick, M.
690 Sienkiewicz, and J. Woollen (2011), MERRA: NASA's modern-era retrospective analysis
691 for research and applications. *J Climate, 24*: 3624–3648. doi:10.1175/JCLI-D-11-00015.1.
692 Rémillard, J., P. Kollias, E. Luke, and R. Wood (2012), Marine Boundary Layer Cloud
693 Observations in the Azores, *J. Climate, 25*, 7381–7398.
694 doi: http://dx.doi.org/10.1175/JCLI-D-11-00610.1
695 Savic-Jovcic, V., and B. Stevens (2008), The structure and mesoscale organization of
696 precipitating stratocumulus, *J. Atmos. Sci., 65,* 1587–1605.
697 Slingo, A. (1990) Sensitivity of the Earth's radiation budget to changes is low clouds, *Nature,*
698 *343,* 49–51.
699 Soden, B., and G. Vecchi (2011), The vertical distribution of cloud feedback in coupled ocean-
700 atmosphere models, *Geophys. Res. Lett., 38,* L12704, doi:10.1029/2011GL047632.
701 Stanfield, R., X. Dong, B. Xi, A. Gel Genio, P. Minnis, and J. Jiang (2014), Assessment of
702 NASA GISS CMIP5 and post CMIP5 Simulated Clouds and TOA Radiation Budgets Using
703 Satellite Observations: Part I: Cloud Fraction and Properties, *J. Clim.,* doi:10.1175/JCLI-D-
704 13-00588.1
705 Stevens, B., W. R. Cotton, G. Feingold, and C.-H. Moeng (1998), Large-eddy simulations of
706 strongly precipitating, shallow, stratocumulus-topped boundary layers, *J. Atmos. Sci.,* 55,
707 3616–3638.

708 Troyan, D. (2012), Merged Sounding Value-Added Product, *Tech. Rep.,* DOE/SC-ARM/TR-
709 087.
710 vanZanten, M. C., B. Stevens, G. Vali, and D. Lenschow (2005), Observations of drizzle in
711 nocturnal marine stratocumulus. *J. Atmos. Sci., 62,* 88–106.
712 Wang, H., and G. Feingold (2009), Modeling mesoscale cellular structures and drizzle in marine
713 stratocumulus. Part I: Impact of drizzle on the formation and evolution of open cells, *J.*
714 *Atmos. Sci., 66,* 3237–3255.
715 Wang L-P, O. Ayala, S. E. Karsprzak, W. W. Grabowski (2005), Theoretical formulation of
716 collision rate and collision efficiency of hydrodynamically interacting cloud droplets in
717 turbulent atmosphere. *J. Atmos. Sci. 62*: 2433–2450.
718 Warren, S. G., C. J. Hahn, J. London, R. M. Chervin, and R. L. Jenne (1986), Global distribution
719 of total cloud cover and cloud types over land, NCAR Tech. Note NCAR/TN-2731STR,
720 National Center for Atmospheric Research, Boulder, CO, 29 pp. 1 200 maps.
721 Warren, S. G., C. J. Hahn, J. London, R. M. Chervin, and R. L. Jenne (1988), Global distribution
722 of total cloud cover and cloud types over ocean, NCAR Tech. Note NCAR/TN-3171STR,
723 National Center for Atmospheric Research, Boulder, CO, 42 pp. 1 170 maps.
724 Wielicki, B. A., R. D. Cess, M. D. King, D. A. Randall, and E. F. Harrison (1995), Mission to
725 planet Earth: Role of clouds and radiation in climate, *Bull. Amer. Meteor. Soc., 76,* 2125–
726 2153, doi:10.1175/1520-0477(1995)076,2125:MTPERO.2.0.CO;2.
727 Wood, R. (2005a), Drizzle in stratiform boundary layer clouds. Part I: Vertical and horizontal
728 structure*, J. Atmos. Sci., 62,* 3011–3033.
729 Wood, R. (2005b), Drizzle in stratiform boundary layer clouds. Part II: Microphysical aspects, *J.*
730 *Atmos. Sci., 62,* 3034–3050.

731 Wood, R. (2006), Rate of loss of cloud droplets by coalescence in warm clouds, *J. Geophys.*
732 *Res., 111,* D21205, doi:10.1029/2006JD007553.
733 Wood, R. (2007), Cancellation of aerosol indirect effects in marine stratocumulus through cloud
734 thinning, *J. Atmos. Sci., 64,* 2657–2669.
735 Wood, R. (2012), Stratocumulus Clouds, *Mon. Wea. Rev., 140*, 2373–2423.
736 doi: http://dx.doi.org/10.1175/MWR-D-11-00121.1
737 Wood, R. and D. Hartmann (2009), Spatial variability of liquid water path in marine low cloud:
738 the importance of mesoscale cellular convection, *J. Climate, 19*, 1748-1764. doi:
739 http://dx.org/10.1175/JCLI3702.1.
740 Wood, R., T. Kubar, and D. Hartmann (2009), Understanding the importance of microphysics
741 and macrophysics for warm rain in marine low clouds. part II: heuristic models of rain
742 formation, *J. Atmos. Sci., 66,* 2973–2990.
743 Wood, R., M. Wyant, C. S. Bretherton, J. Rémillard, P. Kollias, J. Fletcher, J. Stemmler, S. de
744 Szoeke, S. Yuter, M. Miller, D. Mechem, G. Tselioudis, J. C. Chiu, J. A. L. Mann, E. J.
745 O'Connor, R. J. Hogan, X. Dong, M. Miller, V. Ghate, A. Jefferson, Q. Min, P. Minnis, R.
746 Palikonda, B. Albrecht, E. Luke, C. Hannay, and Y. Lin (2015), Clouds, aerosols, and
747 precipitation in the marine boundary layer: An arm mobile facility deployment, *Bull. Am.*
748 *Meteorol. Soc., 96(*3*),* 419–440.
749 Woods, J. D. (1969), On Richardson's number as a criterion for laminar-turbulent-laminar
750 transition in the ocean and atmosphere. *Radio Sci., 4,* 1289–1298,
751 doi:10.1029/RS004i012p01289.
752 Wu, P., X. Dong and B. Xi (2015), Marine boundary layer drizzle properties and their impact on
753 cloud property retrieval, *Atmos. Meas. Tech., 8,* 3555–3562. doi: 10.5194/amt-8-3555-2015.

754 Xue, H., G. Feingold, and B. Stevens (2008), Aerosol effects on clouds, precipitation, and the
755 organization of shallow cumulus convection. *J. Atmos. Sci., 65,* 392–406.
756 Yoo, H., and Z. Li (2012), Evaluation of cloud properties in the NOAA/NCEP Global Forecast
757 System using multiple satellite products. *Climate Dyn., 39,* 2769–2787,
758 doi:10.1007/s00382-012-1430-0.
759 Yoo, H., and Z. Li, Y.-T. Hou, S. Lord, F. Weng, and H. W. Barker (2013), Diagnosis and
760 testing of low-level cloud parameterizations for the NCEP/GFS using satellite and ground-
761 based measurements. *Climate Dyn., 41,* 1595–1613, doi:10.1007/s00382-013-1884-8.
762

763 Table 1. Dates of all 11 cases and their corresponding types. Numbers shown are directional
764 shears (d(dir)/dz) and speed shears (dV/dz) in the vertical direction and the averages of the lower
765 tropospheric stability (LTS) over a 5° × 5° box centered at the Azores.

Date	Type	d(dir)/dz (deg m^{-1})	dV/dz (m s^{-1} m^{-1})	LTS (K)
20090917	I	0.12	0.009	20.0
20091103	I	0.12	0.014	20.9
20100614	I	0.12	0.012	22.3
20100616	I	0.10	0.013	23.1
20100727	I	0.39	0.008	19.4
20101108	I	0.16	0.010	24.0
20091122	II	0.08	0.003	18.2
20100412	II	0.02	0.004	16.6
20100413	II	0.03	0.004	15.9
20100831	II	0.05	0.006	19.0
20101111	II	0.08	0.006	19.1

766

767

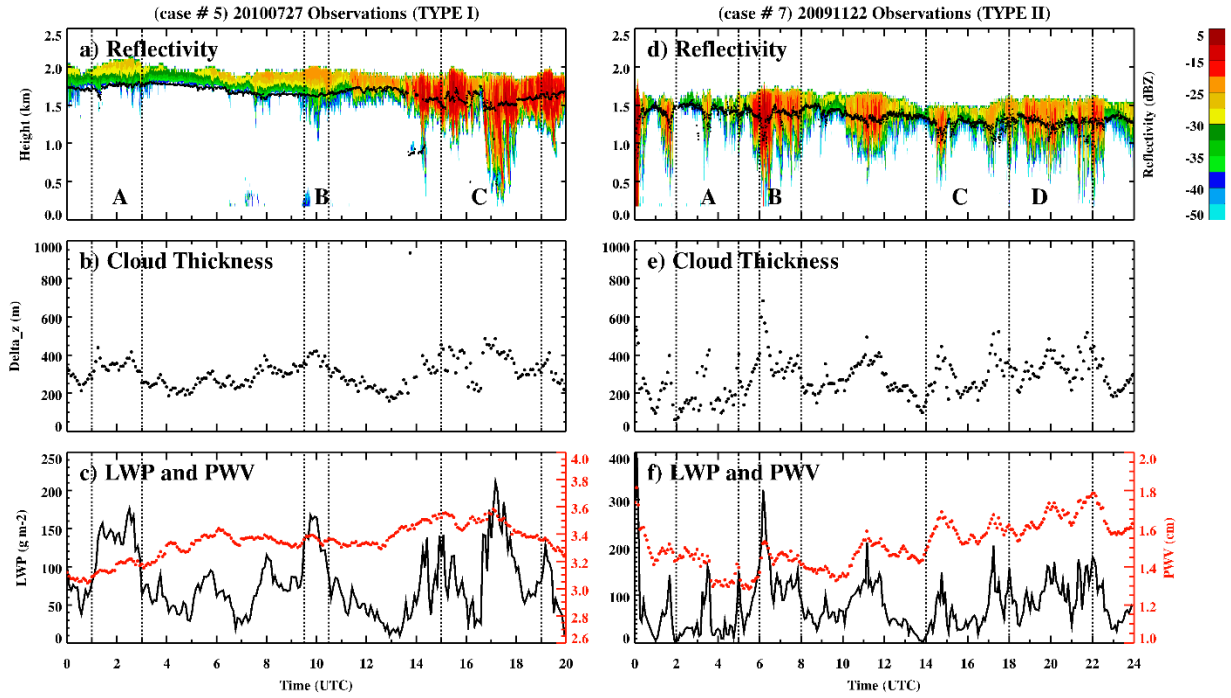

Figure 1. Left column: time series of observations of (a) WACR reflectivity (contour) imposed with CEIL cloud base height (black dots), (b) cloud thickness and (c) liquid water path (*LWP*, black line) and precipitable water vapor (*PWV,* red dots) for the type I case on 27 July 2010 which corresponding to case # 5 in Figure 10. The right column is the same as left but for the type II case on 22 November 2009 and corresponding to case # 7 in Figure 7. Periods noted as A, B, C, and D corresponding to the time periods that are shown in Figures 3, 5 and 9.

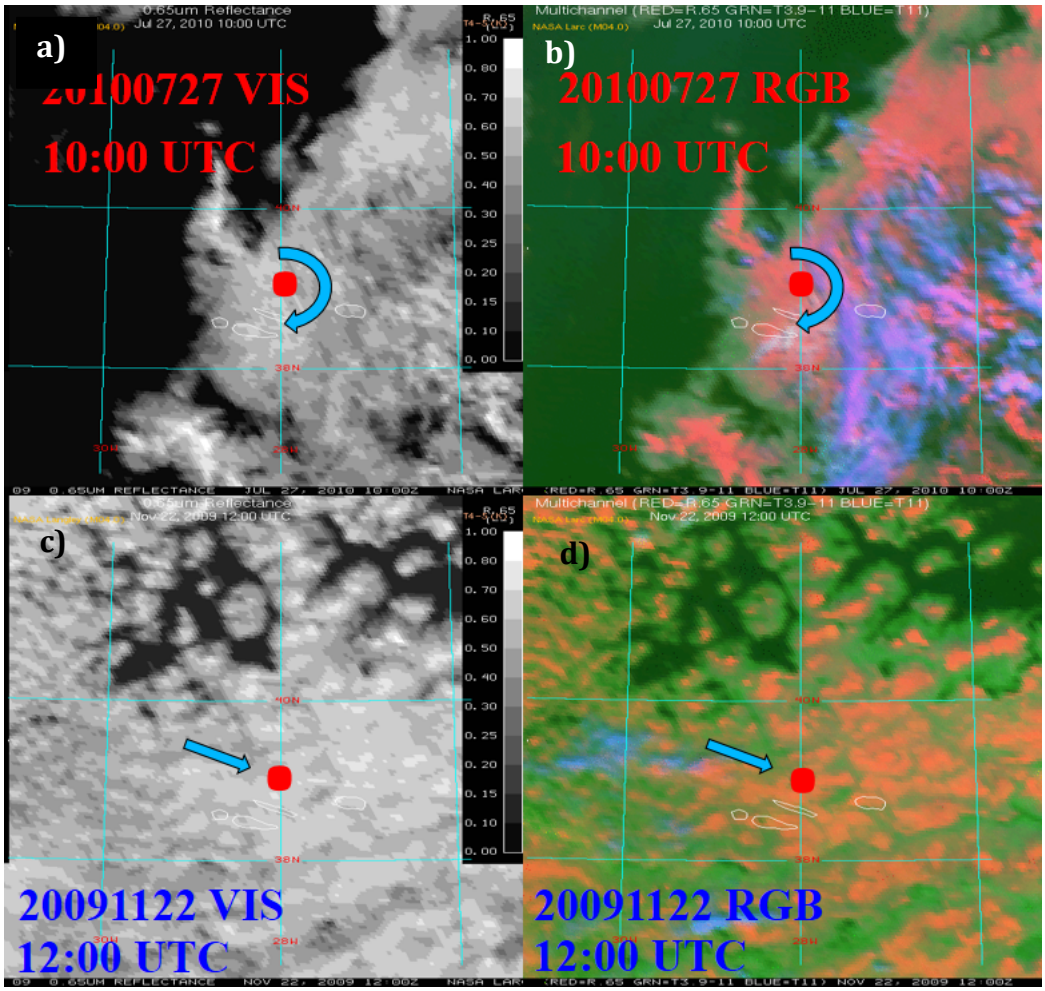

Figure 2: Meteosat-9 visible (left column) and RGB images (right column) over a 6° × 7° box at 10:00 UTC for 27 July, 2010 case (panels a) and b)) and 12:00 UTC for 11 November, 2009 case (panels c) and d)). Red dots denote the location of the Azores, arrows represent the cloud moving direction deduced from consecutive hourly RGB images.

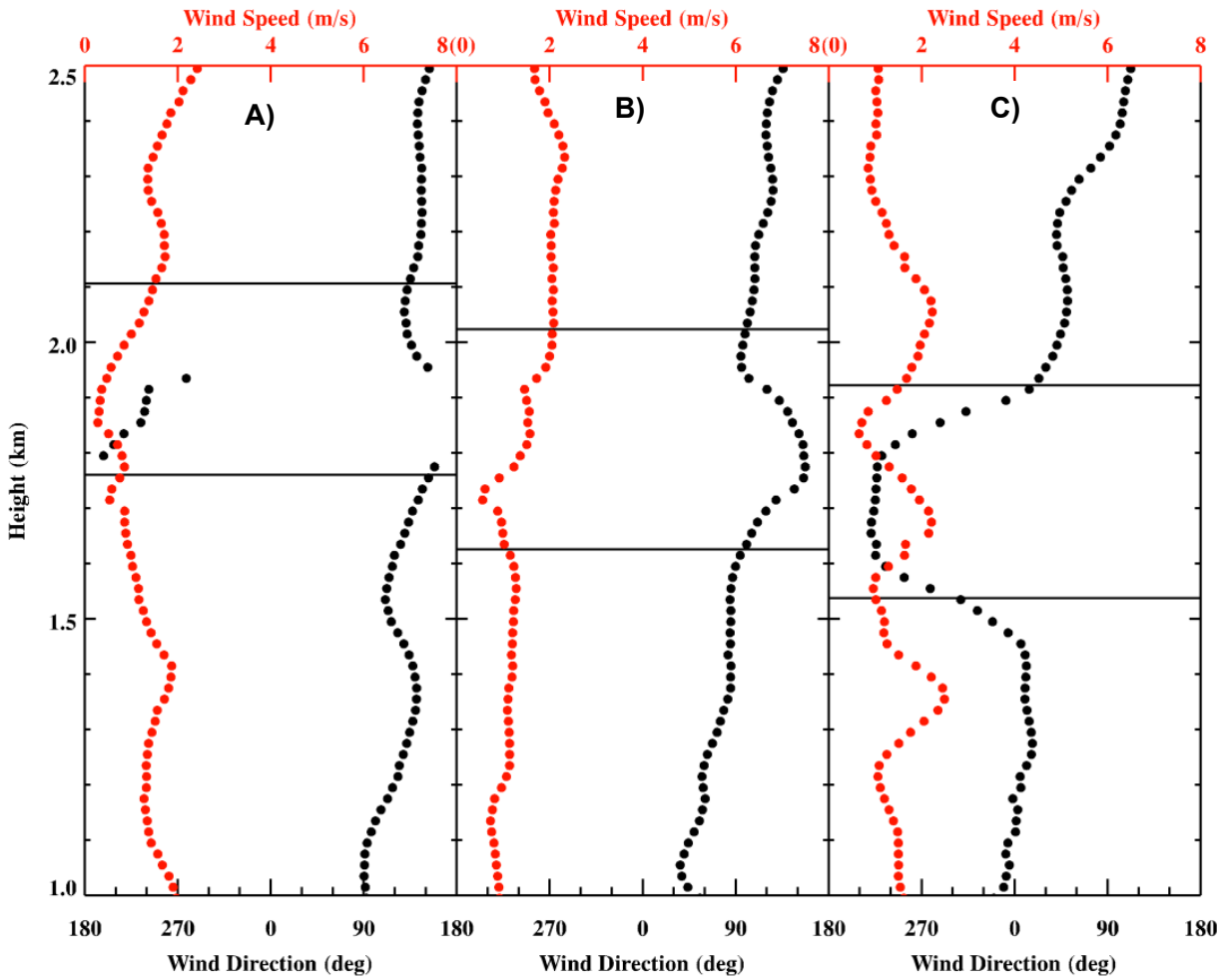

Figure 3. Wind speed (red dots) and wind direction (black dots) from ARM merged soundings for selected periods on 27 July 2010. The three panels correspond to the average speed and direction profiles of three selected time periods (A) 01:00 to 03:00 UTC, (B) 09:30 to 10:30 UTC and (C) 15:00 to 19:00 UTC. Black solid lines represent the mean cloud top and base heights for each time period.

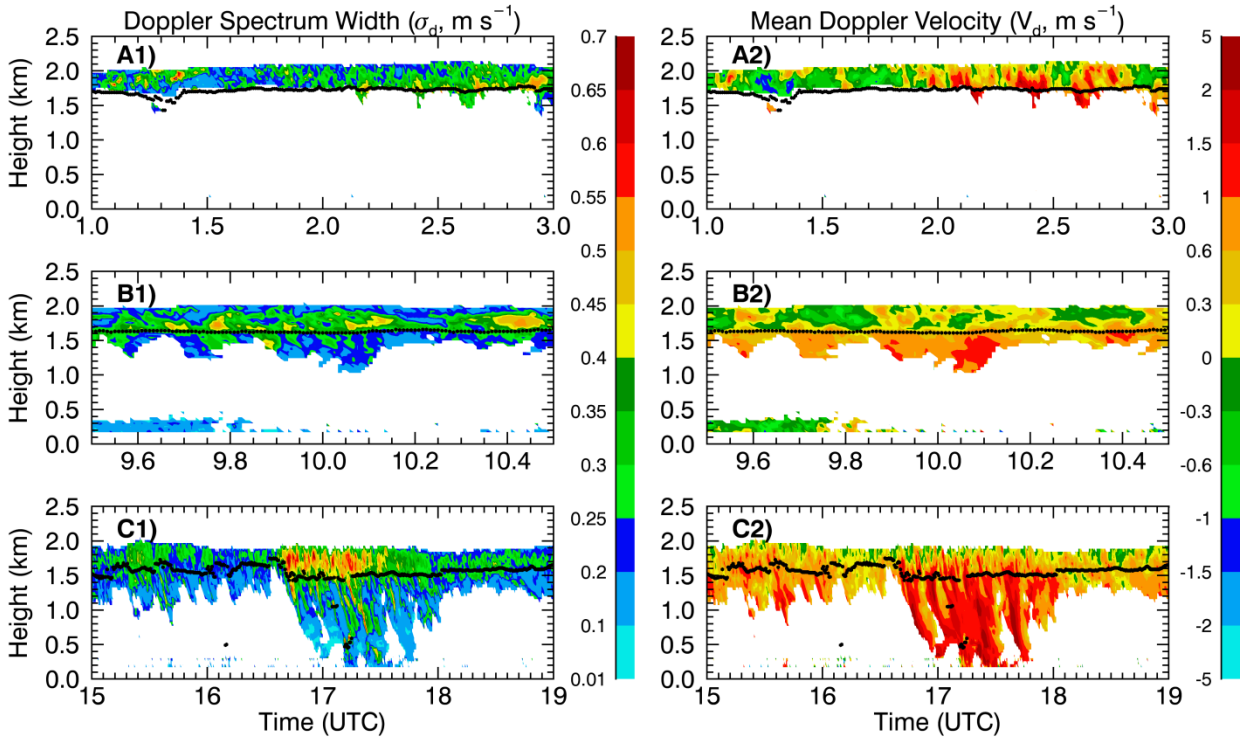

800

801 **Figure 4.** Doppler spectrum width (σ_d, left column) and velocity (V_d, right column) for three
802 selected periods (A) 01:00 UTC to 03:00 UTC, (B) 09:30 UTC to 10:30 UTC and (C) 15:00
803 UTC to 19:00 UTC on 27 July 2010. Black dots indicate the cloud base height, large (small) σ_d
804 values represent broad (narrow) cloud droplet size distributions (DSDs), and positive (negative)
805 V_d values represent downward (upward) motion of cloud droplets.
806

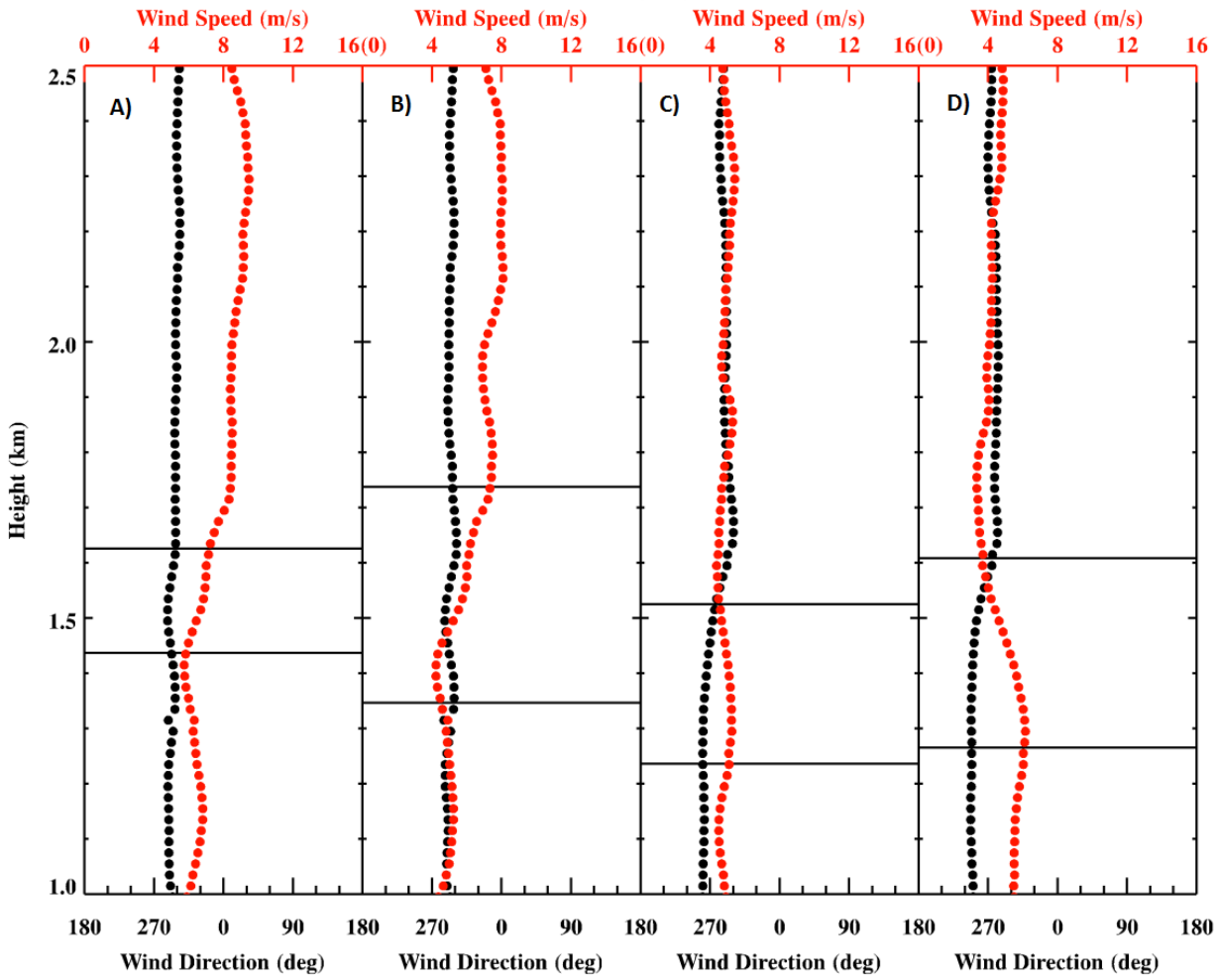

807

808 **Figure 5.** Same as Figure 3 except for the type II case on 22 November 2009. The panels
809 represent the four selected time periods (A) 02:00 to 05:00 UTC, (B) 06:00 to 08:00 UTC, (C)
810 14:00 to 18:00 UTC and (D) 18:00 to 22:00 UTC on 22 November 2009.

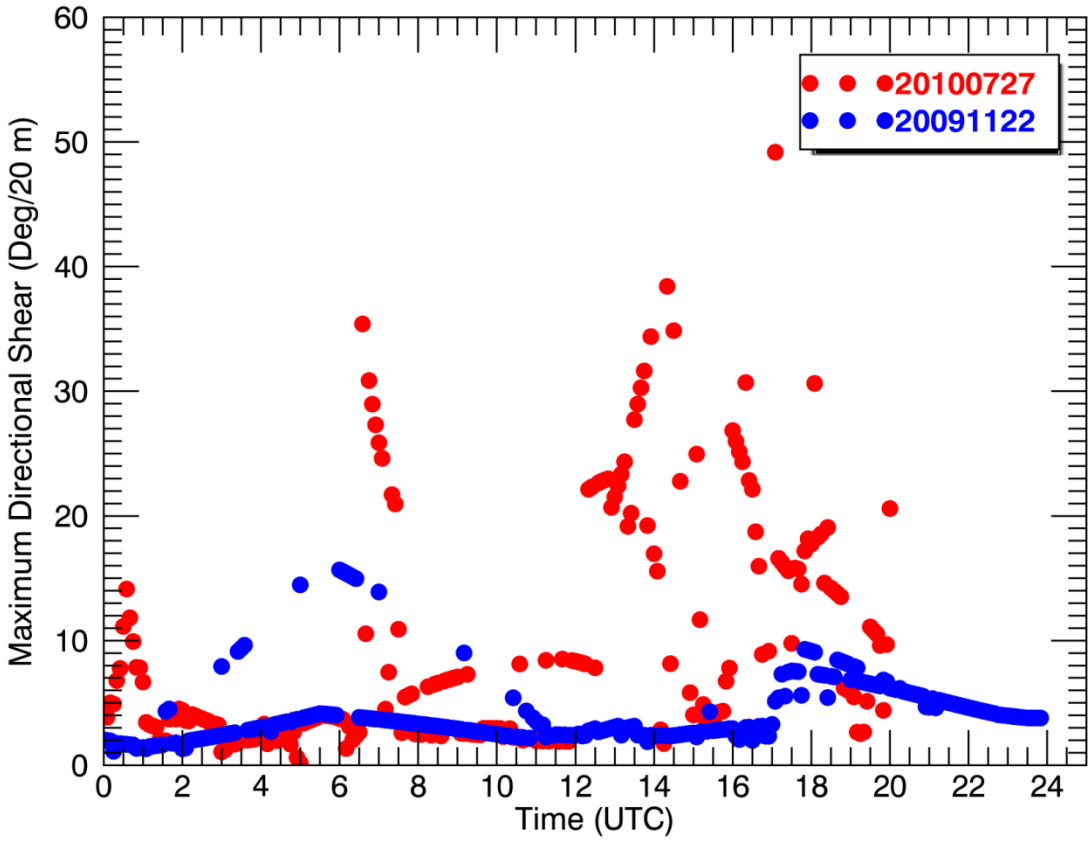

811

812 **Figure 6.** Time series of maximum wind directional shear within the cloud layer for the selected
813 type I case (27 July 2010, red dots) and type II case (22 November 2009, blue dots).

814

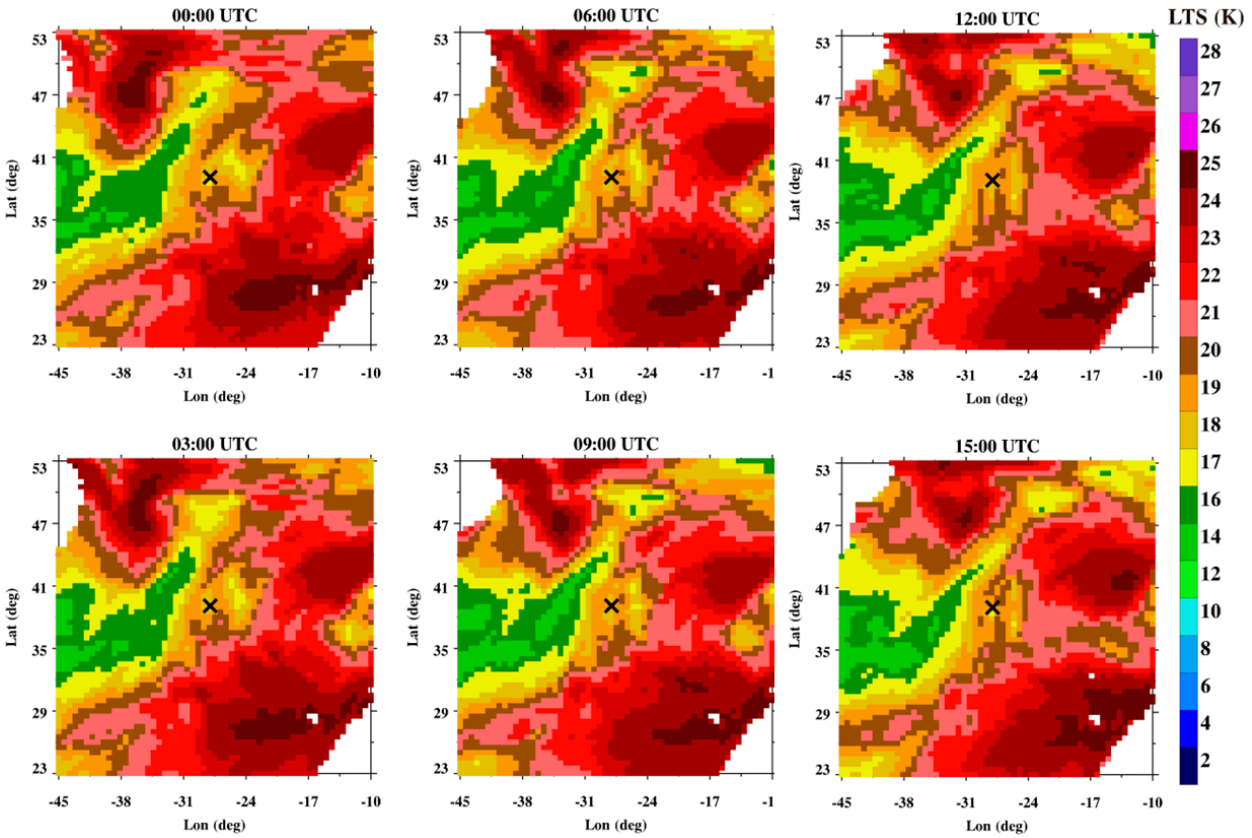

Figure 7. Lower tropospheric stability (LTS) every three hours on 27 July 2010 (type I) calculated from MERRA-2 reanalysis data. The specific time is shown above each panel. Black crosses represent the location of Azores. White areas are due to missing values in surface temperature in MERRA-2 data.

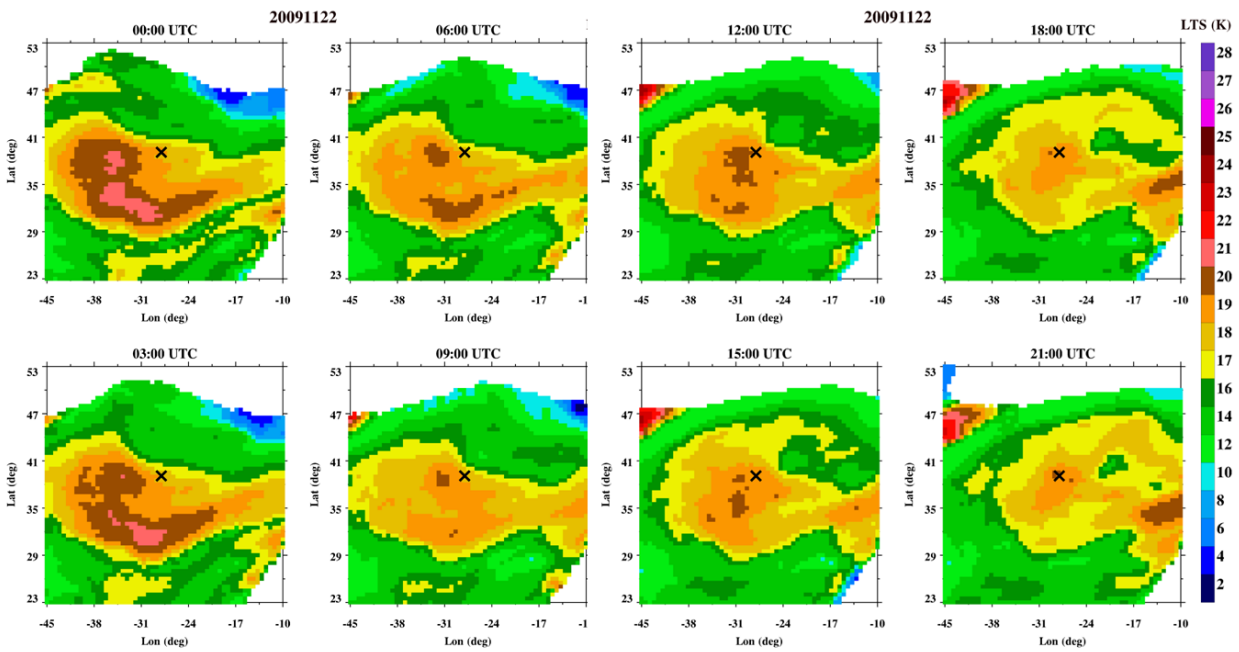

821

822 **Figure 8.** Same as Figure 7 except for 22 November 2009 (type II) and extending to 21:00 UTC.

823

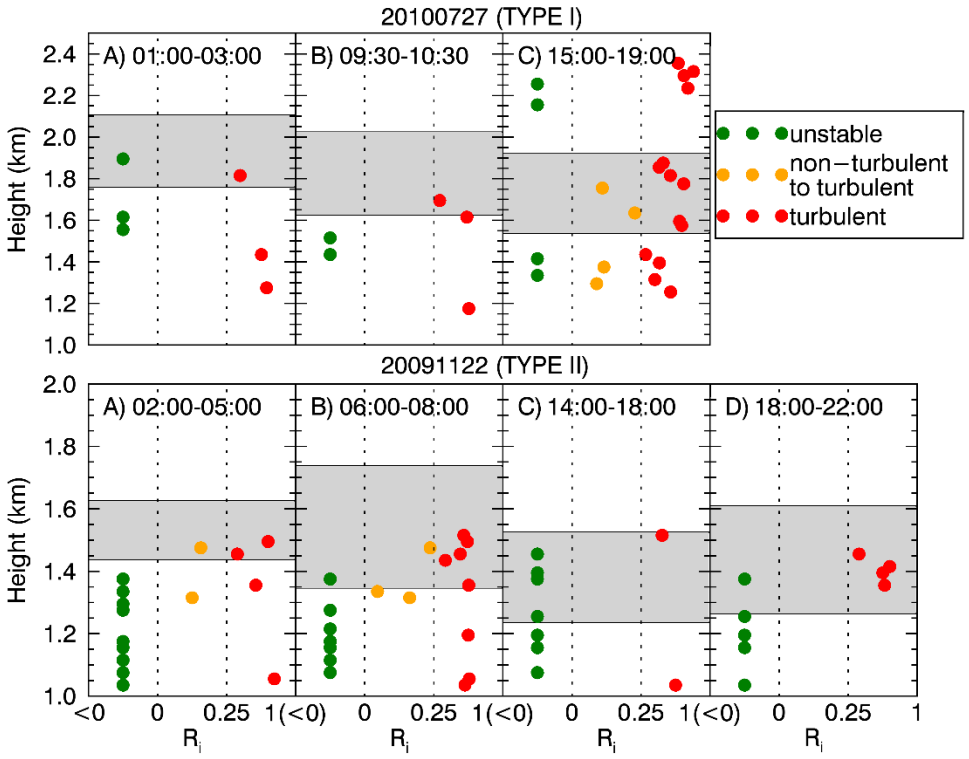

824

825 **Figure 9.** Mean gradient Richardson number (R_i) profiles for the selected periods in Figures 3
826 and 5. Upper panels are for the type I case (20100727) and lower panels are for the type II case
827 (20091122). Each period labelled as A, B, C, and D corresponding to the periods shown in
828 Figures 1, 3, and 5. The shaded areas bounded with solid lines represent the mean cloud layers
829 during each period. Green dots indicate statically unstable, orange dots represent the transition of
830 non-turbulent flow to turbulent flow and red dots indicate that the air is turbulent. Note that the
831 negative values are not plotted as their real values.
832

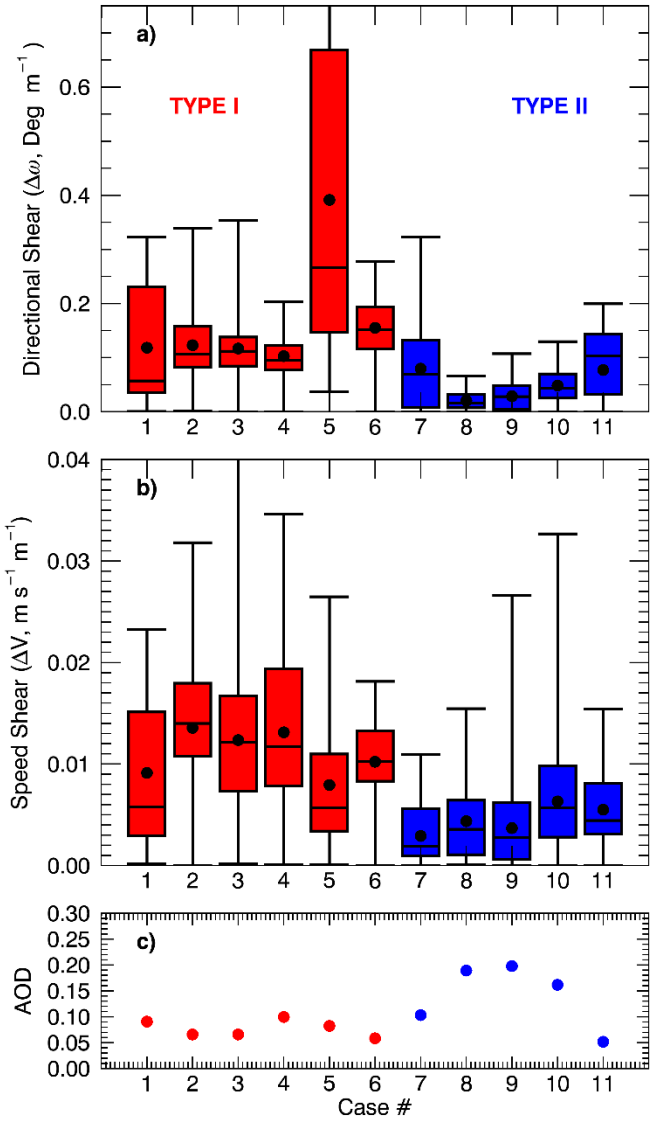

833
834 **Figure 10.** (a) Wind directional shear (Δω), (b) speed shear (ΔV) and (c) aerosol optical depth
835 (AOD) statistics within 100 m above and below the cloud top for all 11 cases. Red and blue
836 boxes represent type I and type II cases, respectively. Horizontal lines represent minimum, lower
837 quartile, median, upper quartile, and maximum values from lower to the upper. Black dots
838 denote the mean values.
839
840

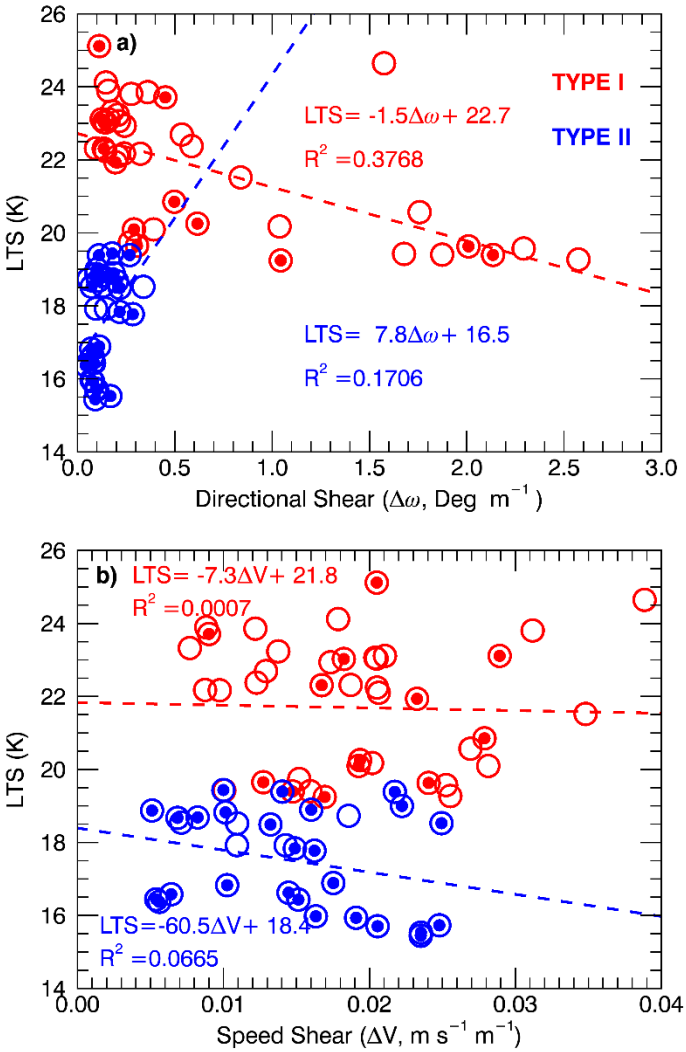

841

842 **Figure 11.** Relationships between 5° × 5° box average of the lower tropospheric stability (LTS)
843 and (a) directional shear (Δω) and (b) speed shear (ΔV) within the cloud layers for the 11
844 selected cases. Each circle represents the mean state for three hours. Red and blue circles
845 represent type I and type II cases, respectively. Circles with solid centers denote drizzling
846 periods. Also shown are the linear regression lines and correlation coefficients (R^2).
847